Pontificia Universidad JAVERIANA Bogotá

Univ. Sci. 30 : 40–64, 2025
doi: 10.11144/Javeriana.SC30.isab

ORIGINAL ARTICLE

In silico antimalarial bioprospecting of neem (*Azadirachta indica*) quinine-derivative alkaloids

Alfin Hidayat[1], **Mamat Sugianto**[1], **Ali Budhi Kusuma**[1,2], **Lili Suharli**[1], **Adhityo Wicaksono**[3*]

Edited by
Angela Johana Espejo Mojica
editorus@javeriana.edu.co

1. Department of Biotechnology, Faculty of Life Sciences and Technology, Sumbawa University of Technology, Jl. Raya Olat Maras Batu Alang, Sumbawa 84371, Indonesia
2. Indonesian Centre for Extremophile Bioresources and Biotechnology (ICEBB), Faculty of Life Sciences and Technology, Sumbawa University of Technology, Jl. Raya Olat Maras Batu Alang, Sumbawa 84371, Indonesia
3. Genomik Solidaritas Indonesia (GSI) Lab, Jl. Sultan Agung No.29, Setiabudi, Jakarta 12980, Indonesia.

*adhityo.wicaksono@gmail.com

Received: 24-04-2024
Accepted: 30-02-2025
Published online: 01-04-2025

Citation: Hidayat A, Sugianto M, Budhi A, Suharli L, Wicaksono A. *In silico* antimalarial bioprospecting of neem (*Azadirachta indica*) quinine-derivative alkaloids, *Universitas Scientiarum*, 30: 40- 64, 2025
doi: 10.11144/Javeriana.SC30.isab

Funding: n.a.

Electronic supplementary material: supp. 1 y supp. 2

Abstract

Malaria, driven by the protozoan *Plasmodium* spp. and transmitted by *Anopheles* mosquitoes, remains a significant global health threat. With the emergence of chloroquine-resistant malaria, alternative treatments derived from natural compounds are pressing. This study explores neem (*Azadirachta indica*), a Southeast Asian plant, as a source of antimalarial agents. A Liquid Chromatography-Tandem Mass Spectrometry (LC-MS/MS) analysis of a neem leaf extract identified 184 compounds, of which five quinone-derivative compounds were subject to in silico screening against three *Plasmodium falciparum* virulence proteins: Purine nucleoside phosphorylases (PNP), dihydroorotate dehydrogenase (DHODH), and erythrocyte membrane protein 1 (EMP1). Among these five compounds (A-E), compound C emerged as the top candidate, ranking highly in molecular stability (FMO energy gaps), drug-likeness (Lipinski's Rule of 5), bioavailability, and synthetic accessibility. Compound C also exhibited strong binding affinity to PNP and DHODH in molecular docking and dynamics simulations and ranked among the top three for binding free energy in MM/PBSA calculations. However, it lacked predicted antiprotozoal activity in PASS screening, though it shared key enzyme targets with established antimalarial drugs. These findings nominate compound C as a promising candidate for further research as a potential antimalarial agent.

Keywords: Bioinformatics; quinine derivatives; antimalarial drug prospection; pathway prediction; secondary metabolite.

1. Introduction

Malaria is a life-threatening parasitic disease affecting millions worldwide. Malaria parasites infect human erythrocytes triggering cell morphology changes and symptoms such as fever, chills, anemia, and an enlarged spleen [1]. Malaria is spread through the bite of a female *Anopheles* mosquito infected with the parasite *Plasmodium* spp. Five known *Plasmodium* species cause malaria, and two of them, *Plasmodium falciparum* and *Plasmodium vivax*, pose the greatest threats, whereby *P. falciparum* is the deadliest malaria parasite. If left untreated, *P. falciparum* malaria can progress to severe disease and can cause death within 24 hours [2]. In 2021, there were an estimated 247 million malaria cases in 84 malaria-endemic countries, representing an increase of 2 million cases compared to 2020 [2].

Two therapeutic agents against Malaria are chloroquine and artemisinin [3]. Chloroquine is a 4-aminoquinoline class schizonticide against all malaria types in humans. Unfortunately, chloroquine and other antimalarial drug-resistant parasites emerge frequently, threatening treatment efficacy and underscoring the need for alternative therapies with novel action mechanisms [4]. Consequently, drug combinations are given to patients, as in artemisinin

combined therapy (ACT), involving artesunate and mefloquine [5]. Artemisinin kills *P. falciparum* by inducing intracellular free radicals [6, 7], artesunate works on breaking *P. falciparum* DNA double strand [7], and mefloquine kills *P. falciparum* by inhibiting its lactate dehydrogenase thus reducing NADH availability and energy production [8]. However, ACT can only be used in patients with uncomplicated *P. falciparum* infections [9].

Currently, quinine is a widely used antimalarial compound of plant origin; it has a similar nitrogen ring structure to mefloquine [10], which was initially isolated from the cinchona tree (*Cinchona officinalis*) [11], known as "kina tree" in Indonesia. Further alternative treatments from plant origins are needed that are inexpensive to produce with low risk levels. Neem (*Azadirachta indica*) is native to continental Southeast Asia that has been introduced to other regions including South Asia, some parts of Indonesia (Sumatra, Java, and Lesser Sunda Islands), Central Africa, the Caribbean, and some of Central and South American countries [12]. Phytochemical studies on neem leaf revealed its alkaloid, anthocyanin, betacyanin, cardiac glycoside, coumarin, flavonoid, glycoside, phenolic, quinone, steroid, saponin, terpenoid, and tannin contents [13]. In a previous study, a neem leaf extract demonstrated strong activity against *P. falciparum* sexual and asexual forms at a median inhibitory concentration of less than 0.5 mg/mL on continuous cultures within 72 hours [14]. Based on this discovery, neem leaf was considered the main antimalarial compound source addressed in the present study.

This study used neem leaf secondary metabolite data obtained via Liquid Chromatography-Tandem Mass Spectrometry (LC-MS/MS). Quinone-derived compounds were then selected and tested as candidate drugs *in silico*. Quinone-derived compounds were sorted from the total compounds, given their known antimalarial role against *P. falciparum*, as quinone structures are part of quinine and mefloquine. Furthermore, these compounds were tested via docking and molecular dynamics against three plasmodial proteins central to malaria onset: DHODH, PNP, and EMP1. Dihydroorotate Dehydrogenase (DHODH) catalyzes the *de novo* synthesis pathway, which is a key pathway for malaria parasites [15], and it is inhibited by drugs such as isoxazole pyrimidine [16] (here, shortened as IZP). Purine Nucleoside Phosphorylases (PNP) are proteins involved in DNA and RNA formation and energy replenishment, producing enzyme cofactors in metabolic pathways and signal transduction components [17]. In *P. falciparum*, PNP is a common binding target for quinoline drugs, e.g., quinine and mefloquine [18]. Finally, *P. falciparum* Erythrocyte Membrane Protein 1 (EMP1), a protein that plays central roles in *P. falciparum* pathogenicity by adhesion of parasite-infected erythrocytes to the vasculature or tissues of infected individuals [19], was also used.

2. Material and methods

2.1. Plant material sampling and preparation

Mature neem (*A. indica*) leaves were collected from wild-grown trees, approximately 10–12 years old, on Sumbawa Island, Indonesia. These trees were situated in natural sandy soil characteristic of a semi-dryland ecosystem and embedded among the local vegetation, including grass species (*Cyperus rotundus*), small herbs (e.g., *Mimosa pudica* and *Chromolaena odorata*), and some trees (e.g., *Ziziphus mauritiana*). The leaves were taken to the Laboratory of Microbiology, Faculty of Life Sciences and Technology at Universitas Teknologi Sumbawa (Indonesia) and dried at room temperature for three to four days to reduce their moisture content. The dry leaves were ground in a blender to obtain a fine powder, which was then packed into plastic pouches of 100 g

each for transport. Samples were sent for Liquid Chromatography Tandem Mass Spectrometry (LC-MS/MS) analysis in the Forensic Laboratory Center (PUSLABFOR) of the National Police Headquarters (Bogor, Indonesia).

2.2. LC-MS/MS run

To prepare for LC-MS/MS, the dried samples were mixed to form a homogenized solution. The weighed and dry neem leaf powder was mixed in methanol, injecting 6 µL of this solution into the liquid chromatograph (Waters, USA) Electrospray System Ionization [20], positive ion model. A Superco C18 (RP18) column served as the stationary phase, with a methanol-water and acetonitrile-water mixture as the mobile phase. The machine column had a length of 50 mm, an inner diameter of 2.1 mm, and a particle size of 1.8 µm with a flow rate of 0.2 mL/min, operating at 50 ºC for 23.20 minutes.

2.3. LC-MS Data Analysis

LC-MS/MS outputs were processed with MassLynx™ v4.1 (Waters, USA) to assign peak identities and molecular masses. The converted molecular structures were then annotated with the ChemSpider database (http://www.chemspider.com) [21]. LC-MS/MS data interpretation and annotation included assigning compound names, formulation numbers, mass weight, monoisotopic weight, and compound 2D structures. Quinonoid [22] derivatives were selected to assess all potential antimalarial drug candidates, which were assigned Simplified Molecular Input Line Entry System (SMILES) codes for subsequent bioinformatics and computational analyses.

2.4. In silico preparation and metabolite profiling

Selected metabolites SMILES codes were converted to three-dimensional protein database (PDB) formats using the Online SMILES Translator and Structure File Generator (National Institute of Health (NIH)) (https://cactus.nci.nih.gov/translate). SMILES codes fed compound property studies, drug-likeness predictions, and reverse biosynthesis analyses to predict each compound's biosynthesis process. In turn, PDB format compounds served molecular docking and dynamics analyses.

To predict compound drug-likeness profiles, an absorption-digestion-metabolism-and-excretion (ADME) analysis in SwissADME (http://www.swissadme.ch/index.php) [23] was used as the first step. The SMILES input allowed the assessment of the following compound properties: (i) Lipinski's Rules of Five (LRo5) obedience [24]; (ii) bioavailability index, predicting the compound's ability to be available in systemic blood circulation (scored from 0 to 1, whereby zero refers to impossible and one indicates instantaneous availability, only occurring by the aid of intravenous injection) [25]; and (iii) synthetic accessibility index, ranging from 1 (easy to synthesize) to 10 (very hard to synthesize) [26].

As a follow-up to the synthetic accessibility index produced by the SwissADME, the biosynthetic pathway of each compound was predicted with a deep learning analysis provided by the BioNavi-NP online tool (http://biopathnavi.qmclab.com) [27] with SMILES codes as inputs, utilizing built-in libraries (core and extended), and default settings. Lastly, using SwissTargetPrediction (http://www.swisstargetprediction.ch) [28], the compounds were evaluated as protein targets, with a list of all targets, and the compound's possible activity as a drug was predicted using Way2Drug PASS Online (http://www.way2drug.com/passonline) [29] as the second tool for drug-likeness prediction process.

2.5. Electron energy gap calculations for frontier molecular orbitals

All metabolites and controls in PDB format served as input for GaussView v6.0 and Gaussian v09W [30] for electron energy calculations. Compound energy level optimizations were performed with the Avogadro v1.2.0 tool [31], equipped with Open Babel v2.3.90 [32]. Then, energy levels were calculated following density functional theory (DFT) using Beck's three-parameter hybrid model with Lee-Yang-Parr functional (B3LYP), with the following settings: basis set of 6-311G(d,p), ground state condition, and default spin. After simulation, the obtained values of the frontier molecular orbitals (FMO), consisting of the highest occupied molecular orbitals (HOMO) and the lowest unoccupied molecular orbitals (LUMO), were used to determine energy gaps on each compound, including controls, which correlates to molecular kinetic stability.

2.6. Molecular docking preparation and processing

Molecular docking was performed in the PyRx pipeline using the Autodock Vina docking program [35]. Five metabolite and three control ligands were subjected to Open Babel v2.3.90 [32] for energy minimization and converted to ready-to-dock ligands. Three protein receptors were selected: (i) purine nucleoside phosphorylase (PNP) (PDB ID: 5ZNC) with quinine as the control drug (HMDB: HMDB0014611) [18]; (ii) dihydroorotate dehydrogenase (DHODH) (PDB ID: 6GJG), a protein of *P. falciparum* targeted for triazolopyrimidine class inhibitor (DSM265) [16], hence isoxazole pyrimidine was used for control (SMILES: CC1=NC(NC2=CC=C(C=C2)C(F)(F)F)=C2C=NOC2=N1); and (iii) erythrocyte membrane protein 1 (EMP1) (PDB ID: 6S8U), a virulence protein exported to the surface of *P. falciparum* parasitized erythrocytes during severe malarial infections. This protein remodels the erythrocyte surface with an EMP-1 knob-like structure, which serves as the interaction point with the intercellular adhesion molecule 1 (ICAM1) [19]. Thus, this docking procedure sought to block the binding site. Following the ligand preparation, the ligands (and the receptors' respective control) were docked to the receptor proteins via multiple ligand-docking procedures on each protein, using specific search spaces and dimensions (Supp. Table 1). The resulting ligands' binding affinities (in kcal/mol) of the least root-mean-squared deviation (RMSD) (RMSD = 0 Å) were listed and compared.

2.7. Molecular dynamics and MM/PBSA

Molecular dynamics simulations proceeded using the GROMACS package [36] with the SiBioLead pipeline (https://sibiolead.com). All receptor-ligand complexes (as shown in Table 1) were simulated under an AMBER99SB force field, an octahedron water box, with water simulated with a Simple Point Charge (SPC) model and a water box charge neutralized using 0.15 M NaCl. The receptor-ligand complexes were first processed for energy minimization with 5.000 steps of the steepest descent integrator. The equilibration setting was a constant number of atoms, volume, and temperature (NVT) per a steady number of atoms, pressure, and temperature (NPT) (NVT/NPT) under a temperature of 300 K, 1 bar of pressure, and a "Leap-frog" integrator. Molecular dynamics simulations run for 50 ns, with 1000 frames per simulation. Simulations produced the following data: root-mean-squared deviations (RMSD) for each receptor-ligand complex and every single protein (later used for control), root-mean-square fluctuation (RMSF) of the protein receptor under ligand influence, and hydrogen bonds between the protein receptor and its ligand. RMSFs helped to detect if the receptor protein amino acid residues were stable or fluctuating less than 3 Å of the total number of amino acid residues [20].

Additionally, the molecular mechanics Poisson-Boltzmann surface area (MM/PBSA) add-on protocol for GROMACS [37] served to determine receptor-ligand energy profiles and estimate binding free energies ($\Delta G_{\text{binding}}$). Subsequently, the obtained energy profiles were compared across all compounds and molecular docking results.

The binding free energy ($\Delta G_{\text{binding}}$; in kcal/mol, see Eqs. 1–3) arises from the sum of the molecular mechanic energy in a gas phase, obtained from the sum of ΔE_{MM} and ΔG_{solv} (Eq. 1), whereby ΔE_{MM} is the molecular mechanic potential energy, arising from the sum of the van der Waals (ΔE_{vdw}) and electrostatic (ΔE_{ele}) interactions (Eq. 2); and ΔG_{solv}, the electrostatic solvation energy, is the sum of the polar energy contribution calculated via the Poisson-Boltzmann model (ΔG_{PB}) and the non-polar contribution of the surface area (ΔG_{SA}) [38] (Eq. 3).

$$\Delta G_{\text{binding}} = \Delta E_{\text{MM}} + \Delta G_{\text{solv}} \quad (1) \tag{1}$$

$$\Delta E_{\text{MM}} = \Delta E_{\text{vdw}} + \Delta E_{\text{ele}} \quad (2) \tag{2}$$

$$\Delta G_{\text{solv}} = \Delta G_{\text{PB}} + \Delta G_{\text{SA}} \quad (3) \tag{3}$$

3. Results

3.1. Metabolite detection and selection

Of the 184 compounds detected via LC-MS/MS and identified using the ChemSpider database (see Supp. Table 1, which can be provided upon request), five quinone derivatives were selected based on structural relevance to known antimalarial agents (**Table 1**).

The molecular predictions of the five selected compounds, as obtained through conversion to PDB format, are shown in **Fig.1** (a-e) respectively. Likewise, the formulae of the two control compounds, quinine and isoxazole pyrimidine are shown in Fig. 1 (f and g).

3.2. FMO energy gap profiles

Energy gaps (ΔE) between each molecule's FMOs, HOMO and LUMO, were calculated to compare the compound activity profile to the control compounds and are shown in **Fig. 2**. The orbital profiles of the compounds revealed the map of electron distributions on HOMO and LUMO.

Control drug FMO energy gaps were notably higher than those of the five test compounds (**Fig. 3**). Of these five compounds, compounds A, E, and C are the ones with the broadest energy gaps, while compound D possesses the narrowest energy gap. This profile suggests compound A possesses the highest kinetic stability to form a stable chemical bond, while compound D might create the least stable bond. To find out the interactions between compounds and receptor proteins, molecular docking, and molecular dynamic analyses were subsequently conducted. These resulted in predictions on static (docking) and time-dependent processes (dynamics) for the studied compounds.

Table 1. Selected quinone-derived metabolites.

Compound Code	Formula	Compound Name	Peak	ChemSpider ID	Average Weight (Da)	Monoisotopic Weight (Da)
A	$C_{11}H_9NO_2$	6-Methoxy-8-quinolinecarbaldehyde	3.98	25069090	187.195	187.063
B	$C_{33}H_{26}N_2O_9$	1,9,11,14-Tetrahydroxy-7-methoxy-10-methyl-8,13-dioxo-3-(1,2,3,4-tetrahydro-2 -quinazolinyl)-5,6-dihydrobenzo[a]tetracene-2-carboxylic acid	5.74	24611442	594.568	594.164
C	$C_{30}H_{31}N_5O_4$	2-Amino-N-[2-(3,4-diethoxyphenyl)ethyl]-1-(3-methoxyphenyl)- 1H-pyrrolo[2,3-b]quinoxaline- 3-carboxamide	8.29	2833819	525.598	525.238
D	$C_{23}H_{18}N_{10}O_2$	N-{4-[7-(2-Furyl)-4-methyl[1,2,4]triazolo[5,1-c][1,2,4]triazin-3-yl]-2-pyrimidinyl}-6-methoxy-4-methyl-2-quinazolinamine	9.02	28624201	466.455	466.161
E	$C_{30}H_{55}ClN_6O$	N-(5-Amino-2-pentanyl)-N'-[4-({4-[(6-methoxy-8-quinolinyl) amino}pentyl)amino)pentyl]-1,4-pentanediamine hydrochloride	18.55	34223155	551.25	550.413

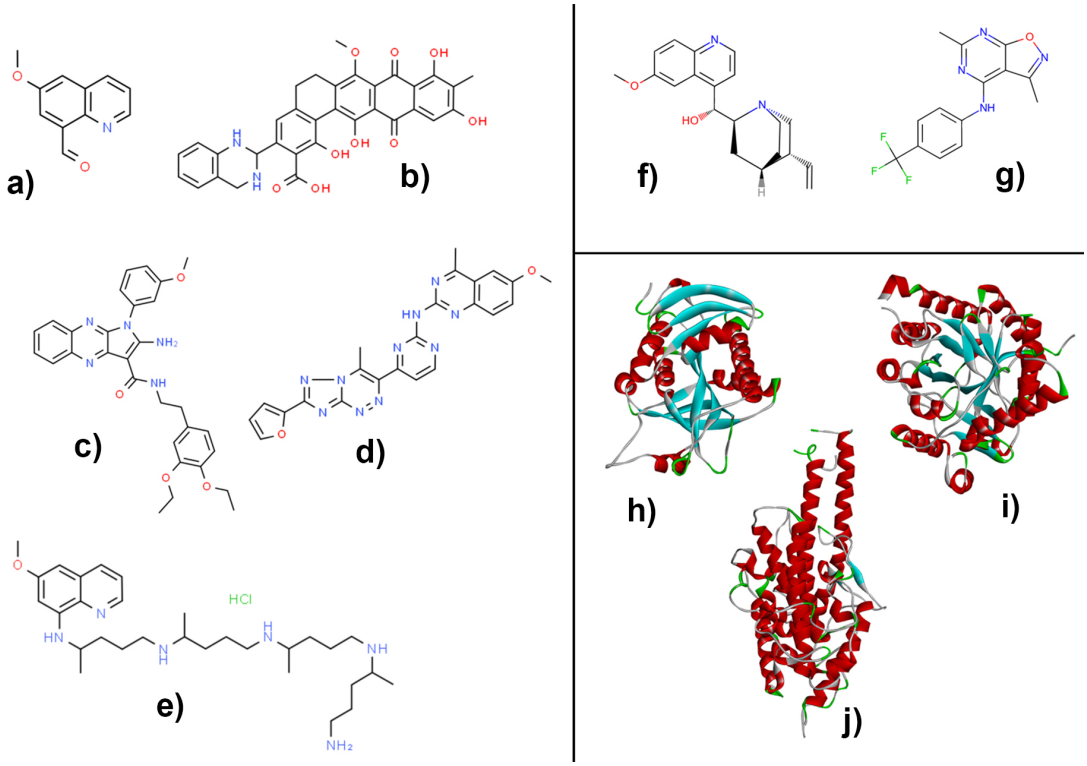

Figure 1. Molecular projections of five selected quinone derivatives, compounds (**a-e**); control drugs: quinine (**f**) and isoxazole pyrimidine (**g**); and the three studied protein receptors: Purine nucleoside phosphorylase (PNP) (**h**), dihydroorotate dehydrogenase (DHODH) (**i**), and erythrocyte membrane protein 1 (EMP1) of *Plasmodium falciparum* (**j**). PNP is the drug target for quinine and DHODH is the inhibitor drug target for isoxazole pyrimidine.

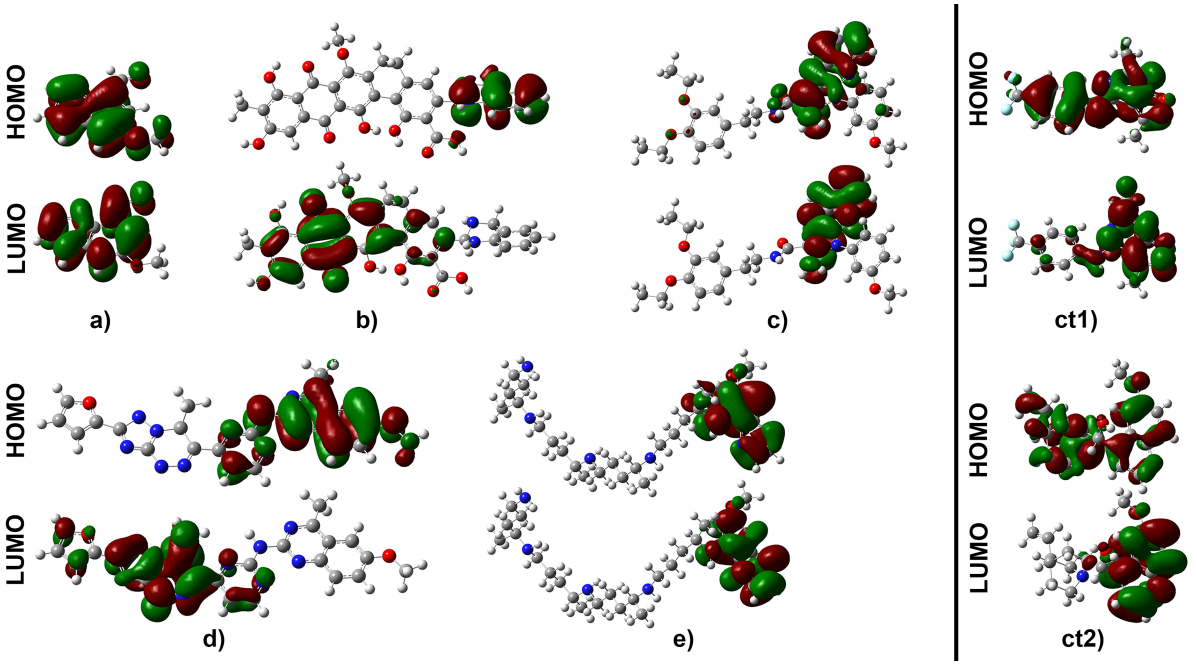

Figure 2. Map of the FMO, consisting of HOMO and LUMO of all compounds (Compound A to E, a-e) and controls (ct1 and ct2).

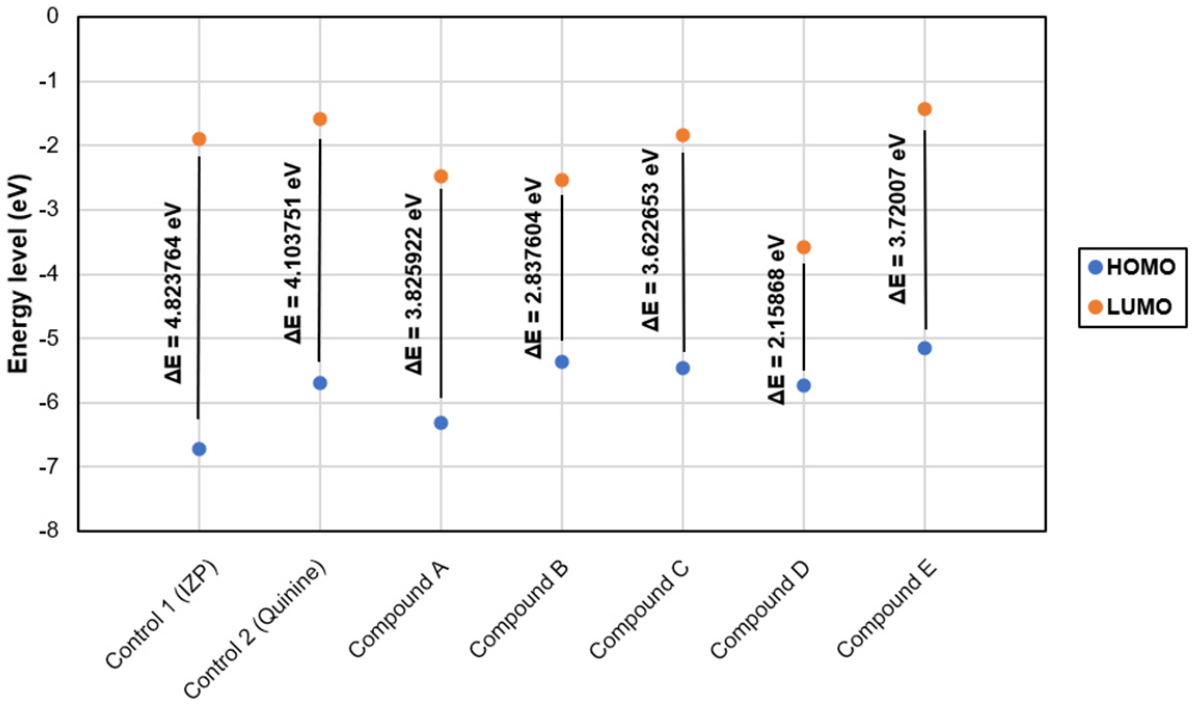

Figure 3. HOMO-LUMO energy gaps of all compounds (controls and test compounds A to E).

3.3. Metabolite prospective drug profiles

Compound characterization via ADME analysis served to assess compound compliance with LRo5 rules and establish its bioavailability and synthetic accessibility profile. **Table 2** provides the feature values for each studded compound. Compound B failed to comply with LRo5 due to its high molecular weight and number of hydrogen acceptor and donor atoms. The other compounds followed the LRo5 even with a single permissible violation. However, compound A did not violate a single LRo5 criterion. In terms of bioavailability, compound B was the least bioavailable, with a value of 0.17, while the rest of the compounds had a bioavailability score of 0.55. In terms of synthetic accessibility, compound E was the hardest to synthesize, while compound A was the simplest. Subsequently, BioNavi-NP was used to confirm each compound's biosynthetic pathways.

Table 2. ADME analysis results for control and studied metabolites.

ID	Molecular Weight (Da)	LRO5	LRO5 Violation?	Bioavailability	Synthetic Accessibility
IZP	294.23	Yes	0	0.55	2.93
Quinine	324.42	Yes	0	0.55	4.34
A	187.19	Yes	0	0.55	1.3
B	594.57	No	3 (1,3,4)	0.17	4.88
C	525.6	Yes	1 (1)	0.55	3.8
D	466.45	Yes	1 (3)	0.55	3.69
E	551.25	Yes	1 (1)	0.55	5.35

LRO5 violation details: (1) MW > 500, (2) MLOGP > 4.15, (3) H acceptor (N or O) > 10, (4) H donor (NH or OH) > 5. Bioavailability: score range: 0 to 1, whereby 0 implies its impossibility to reach the systemic bloodstream and 1 means instantaneous access that is typically done by intravenous injection [25]. Synthetic Accessibility: Range of 1 to 10, 1 is easiest to build and 10 is nearly impossible [26].

The BioNav-NP pathway prediction (Supp. Fig. 1 and Supp. Data 1 provided upon request) tool was employed to check if the SwissADME synthetic accessibility prediction matched pathway prediction (i.e., whether high synthetic accessibility values correlate with high intermediary numbers within the pathway and vice versa), whereby a low score value implies a high likelihood of numerous intermediaries. The intermediary numbers per compound were as follows: Compound A had 3, B, 4; C, 3; D, 2; and E, 2. Implying that compounds D and E had the shortest building path, and compound B had the longest. Of all compounds, only compound E was very likely involved with recognized enzymatic reactions, *e.g.*, pyruvate: ubiquinone oxidoreductase (gene: poxB; MetaNetX ID: MNXR143500; EC: 1.2.5.1; score: 2.9) and succinyl-CoA: acetate CoA-transferase (gene: aarC; MetaNetX ID: MNXR188880; EC: 2.8.3.18; score: 5.1). However, the overall compound scores did not correlate with the previous results on synthetic accessibility values. As for the controls, IZP has nine intermediates, and quinine only has two intermediates.

The PASS results predicted compound activities on certain biological functions, with high probability values representing a high likelihood for the compound to be active within a given function. Of all five studied compounds (**Fig. 4**), only A and E were likely to have specific antiprotozoal and antiplasmodial functions, although none scored higher than quinine. The rest of the compounds were improbable to have activities with these two functions.

The SwissTargetPrediction tool identified the proteins probably targeted by the assessed compounds. Table 4 shows only enzyme targets, and further details are provided in Supp. Data 2 (upon request only). Moreover, Supp. Fig. 2 shows all potential targets. The presence of

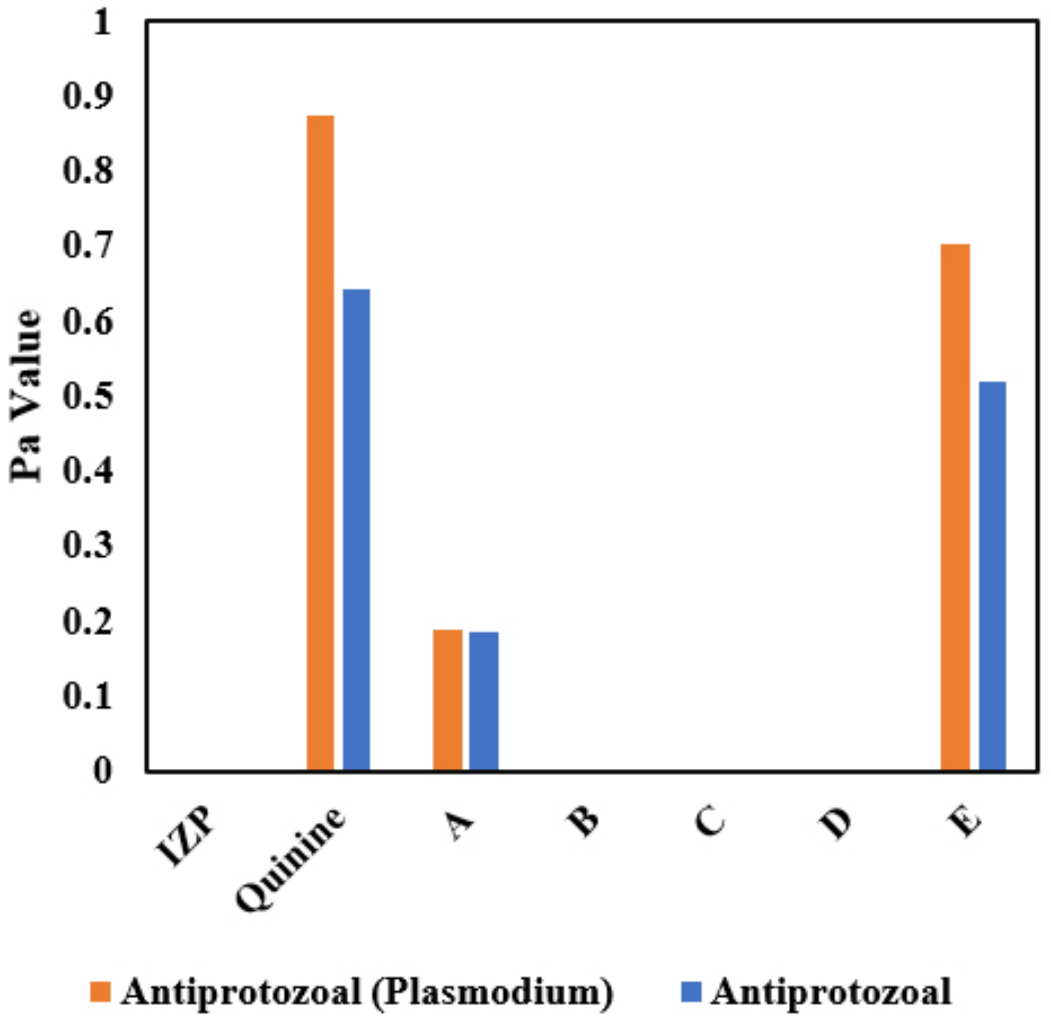

Figure 4. PASS results of the controls and the five metabolites (Compound A to E in X-axis; Table 1) with the probability of being "active" set for antiprotozoal (general) and antiplasmodial activities

shared enzyme targets suggested similarities among the compounds. Compound A targets 13 enzymes (35 %), a kinase (13 %), and a protease (11 %). Compound B targets enzymes of the AG protein-coupled receptor family (26 %), followed by a kinase (19 %), and a lyase (7 %). Compound C targets a kinase (27 %), followed by 18 enzymes (18 %), and a member of the AG protein-coupled receptor family (11 %). Compound D targets a protease (38 %), a member of the AG protein-coupled receptor family (17 %), and multiple enzymes (14 %). Finally, compound E is likely to target a kinase (32 %), a member of the AG protein-coupled receptor family (23 %), and a lyase (9 %).

As for the control compounds, IZP targets a kinase (19 %), receptors of the protein-coupled CG family (15 %), and receptors of the protein-coupled AG family (10 %), whereas quinine targets a kinase (37 %), receptors of the protein-coupled AG family (20 %), and multiple enzymes (6 %).

The studied compounds and controls can share multiple enzyme targets (Supp. Table 2). Compound A and quinine can target the enzyme nitric oxide synthase. Compounds C and D each share one enzyme with IZP: acyl-CoA desaturase and 11-β-hydroxysteroid dehydrogenase,

respectively. Compound A and compound C share one target, glutamine γ-glutamyltransferase. Lastly, compound C shares one target, 6-phosphofructo-2-kinase/fructose-2,6-bisphosphatase 3, with compound D. In conclusion, compounds A, C, and D are more favorable candidates due to their shared enzyme targets with the controls.

3.4. Molecular docking

The static yet flexible structural interactions, as binding affinity energies between the studied compounds with three protein targets as receptors, were tested using molecular docking. Molecular docking tools evaluate rigid or flexible docking regarding ligand insertion protocol, and Autodock Vina uses flexible ligand docking [39]. Targeted against three protein receptors and compared with control ligands (for PNP and DHODH protein targets), compounds B, C, and D surpassed quinone's binding affinity with PNP, and Compounds C and E had stronger binding affinities than IZP with DHODH. Compound C revealed the strongest affinity with these two protein receptors (**Table 3**).

Docked against EMP1, compound D revealed the highest binding among the tested compounds, followed by C and B. All the dominant interactions came from the hydrophobic interactions (van der Waals), and the conventional hydrogen bonds contributed only from one to a maximum of five interactions (on average, two interactions). Only compound D revealed one unfavorable bond (donor-donor interaction). Ultimately, C and D are arguably the best docking compounds (detailed interaction data for the top compounds versus controls, except for EMP1, provided in **Fig. 5**)

3.5. Molecular dynamics and MM/PBSA calculations

Molecular dynamics simulations helped to overcome the limitations of the static interactions predicted with molecular docking. Molecular dynamics uses solvation and time-dependent calculations. Following the 50 ns of simulation runtime with the three protein receptors (**Fig. 6a**), compounds A, B, C, and quinine fluctuated below the protein fluctuation baseline (average protein fluctuation) in PNP. None of the compounds fell below the baseline; however, compound C and IZP came closest to it in DHODH. Compounds A, C, and D were the closest to the baseline in EMP1.

Protein fluctuations remained relatively stable during simulations, with less than 10 % of the residues fluctuating over 0.3 Å of each protein's total residues and all residues fluctuating almost in the same pattern as the average protein baseline in all compound simulations (Fig. 6b). Throughout the simulations, the number of protein-ligand hydrogen bonds fluctuated, and only compounds C and E exhibited the highest and the densest amount of hydrogen bonds per simulation runtime (refer to Supp. Fig. 3). These molecular dynamics simulations revealed compound C as having the best properties of an inhibitory drug compound.

The binding free energies ($\Delta G_{\text{binding}}$) between tested ligands and the protein receptors were estimated using MM/PBSA, revealing that compounds C, D, and E constantly topped energy values with all three protein receptors (**Fig. 7**).

Table 3. Molecular docking results of five tested metabolite ligands on three protein receptors and their essential bonds. Binding affinity in kcal/mol.

Receptor	Ligand	Binding Affinity	H-bonds	Receptor-Ligand Interactions	Unfavorable bonds
PNP (PDB ID: 5ZNC)	Quinine (Control)	-8.2	1 (Asp 206)	10 (Gly23, Asp24, Arg88, Cys92, Gly93, Ser157, Glu182, Pro209, Trp212, Asp218)	
	Compound A	-7.6	1 (Trp212)	8 (Cys92, Gly93, Glu182, Met183, Asp206, Gly207, Cys208, Asp218)	
	Compound B	-8.7	1 (Ser91)	12 (Val22, Gly23, Asp24, Arg88, Ala89, Glu182, Met183, Glu184, Ile204, Leu221, Leu226, Met229)	
	Compound C	-9.3	2 (Ser91, Asp218)	11 (Gly23, Asp24, Gly90, Cys92, Gly93, Glu182, Asp206, Gly207, Cys208, Asn219, Asn220)	
	Compound D	-8.7	1 (Tyr160)	7 (Gly23, Asp24, Val66, Ala89, Asp206, Asp218, Asn219)	
	Compound E	-7.5	2 (Ala89, Ser91)	22 (Val22, Gly23, Asp24, Arg27, Ile31, Val66, Arg88, Gly90, Gly93, Ser157, Met159, Leu170, Glu182, Glu184, Asp206, Gly207, Cys208, Asp218, Leu221, Leu226, Met229, Ile230)	
DHODH (PDB ID: 6GJG)	Isoxazole Pyrimidine (Control)	-9.7	0	5 (Ile237, Leu240, Ile263, Leu531, Met536)	
	Compound A	-7.3	1 (Lys229)	6 (Ala225, Gly226, Cys276, Lys429, The459, Ser477)	
	Compound B	-4.7	0	2 (Ile179, Thr256)	
	Compound C	-11.1	5 (His185, Asn274, Cys276, Ser345, Tyr528)	18 (Leu172, Gly181, Phe188, Ala224, Ala225, Gly226, Thr249, Arg265, Gly277, Asn342, Asn347, Lys429, Asn458, Thr459, Ser477, Ser505, Gly506, Ser529)	
	Compound D	-5.5	3 (Arg265, Asn458, Ser477)	11 (Gly181, Phe188, Gly226, Lys229, Phe264, Cys276, Phe278, Asn342, Ser345, Lys429, Ser529)	1 (Ile263)
	Compound E	-8.7	2 (Ala89, Ser91)	20 (Leu189, Gly192, Leu197, Phe227, Lys229, Cys233, Ile237, Leu240, Arg265, Ile272, Gly277, Phe278, Ser345, Pro246, Asn347, Lys429, Asn458, Thr459, Ser477, Gly535)	
EMP1 (PDB ID: 6S8U)	Compound A	-5	1 (Gly1110)	5 (Ala1104, Phe1108, Ala1109, Thr1111, Gln1121)	
	Compound B	-7.5	1 (Glu1099)	7 (Asp838, Asp840, Lys1096, Gln1103, Thr1111, Ser1112, Gly1115)	
	Compound C	-7.7	2 (Arg1118, Gln1121)	8 (Arg928, Asn974, Glu982, Ser1112, Phe1113, Gly1114, Asp1119, Gln1122)	
	Compound D	-8.8	2 (Phe1113, Gln1121)	8 (Asp758, Ala759, Arg928, Asn974, Ser1112, Gly1114, Asp1119, Gln1122)	
	Compound E	-5.2	1 (Glu1099)	9 (Thr837, Asp840, Asp1095, Lys1096, Glu1098, Gln1103, Ile1106, Gly1114, Gly1115)	

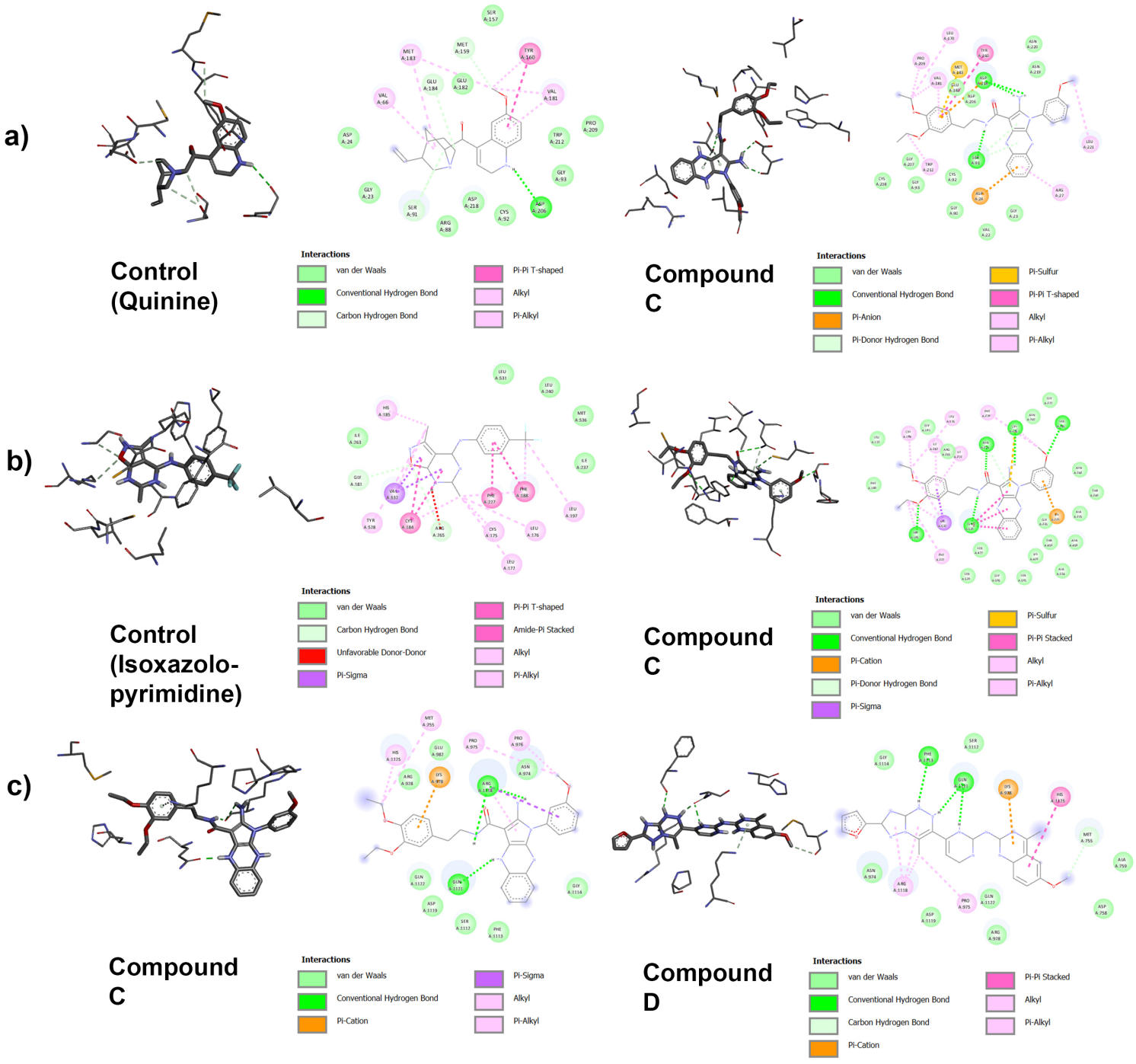

Figure 5. Docking interactions between selected protein receptors and ligands in 3-dimensional view and their respective 2-dimensional map. Protein receptors: **a)** PNP, **b)** DHODH, and **c)** EMP1. Ligands on the left side of a and b are the two control ligands, and the ligands depicted on the right-hand side are the ones with the highest binding affinities. For protein c, the ligand on the left side is Compound C, as this compound held the highest binding affinities while being docked the other proteins (protein a and b), and the ligand on the right is Compound D, ligand with the highest binding affinity for docking simulation with protein C.

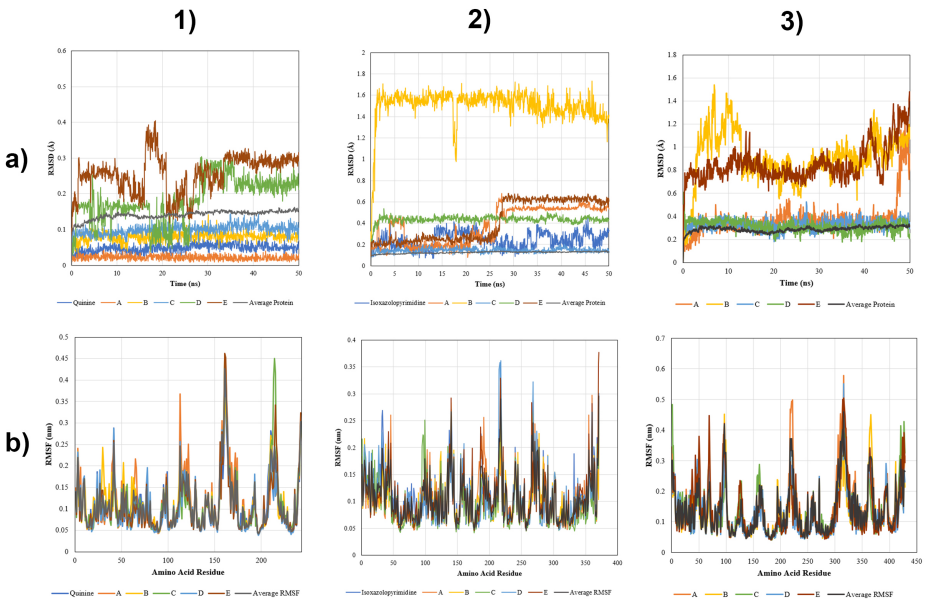

Figure 6. a) RMSD (in Å) and **b)** RMSF (in nm) values of the interactions between five test and two control compounds with three *Plasmodium falciparum* protein receptors: 1) PNP, 2) DHODH, and 3) EMP1. Control compound-to-protein receptor interactions were assessed for given combinations.

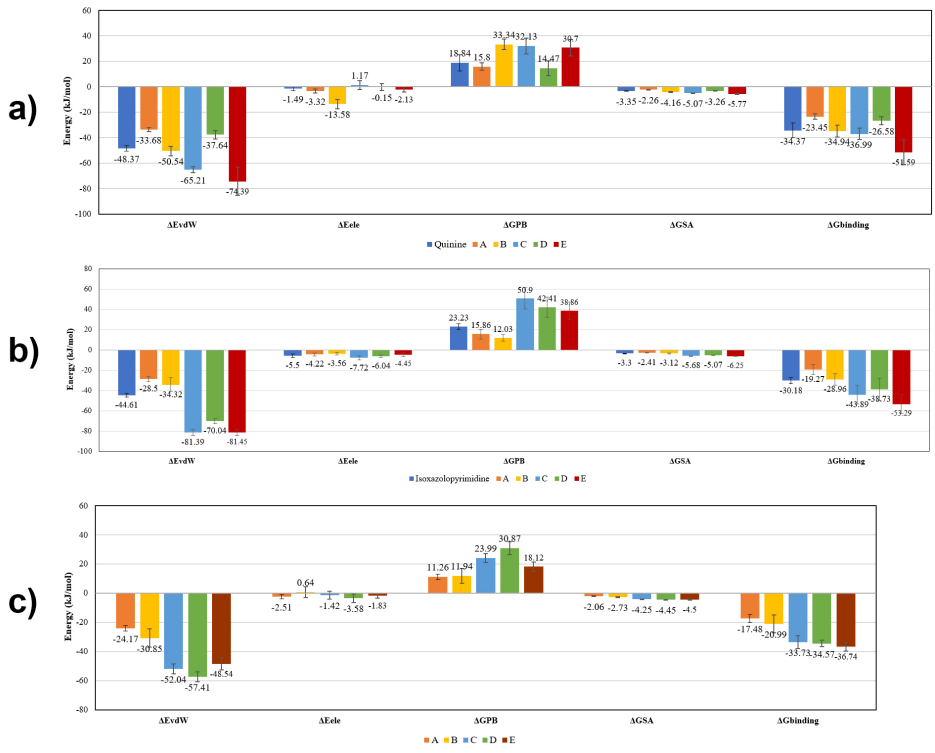

Figure 7. MM/PBSA calculation results, revealing the energy profiles (in Kcal/mol) of the interactions between five metabolites and two controls with three *Plasmodium falciparum* protein receptors: **a)** PNP, **b)** DHODH, and **c)** EMP1. Control compound-to-protein receptor interactions were assessed for given combinations. The error bars indicate the standard deviation value generated from the total simulation.

4. Discussion

4.1. Neem extract and compound characteristics

Neem extract and juice have been tested as antimalarial drug candidates on mice and revealed significant results against *Plasmodium* [40, 42, 43]. The present study evaluated with an *in silico* approach whether quinone-derivative compounds present in neem extract are potential targets of three plasmodial, malaria-related proteins (DHODH, PNP, and EMP1).

In our study, five quinone-derivative compounds, selected from 184 compounds detected via LC-MS on neem extract, were assessed for energy gaps between two types of molecular orbitals, HOMO, as the outermost orbital filled with electrons serves as the electron donor to the LUMO orbital, which is the lowest energy orbital with spaces to accept electrons [44]. In comparison to the control compounds (quinine for PNP and IZP for DHODH), which have the broadest electron energy gaps between HOMO and LUMO (4.104 and 4.824 eV for quinine and IZP, respectively), compounds A, E, and C revealed the broadest energy gaps among the selected compounds, with 3.826 eV, 3.720 eV, and 3.623 eV, respectively (Fig. 3). These ample energy gaps contribute to molecule stability when bonding to the other molecules, which in this case, are the protein amino acid residues.

Following compound drug-likeness profiling with an ADME analysis, focusing on bioavailability and synthetic accessibility (Table 3), compounds A, C, and D obtained the most favorable scores for both features. Bioavailability score values inversely correlate with a drug's molecular mass, with larger molecules generally exhibiting lower bioavailability [45]. Synthetic accessibility, on the other hand, reflects molecular complexity [26]. Compound B obtained the lowest bioavailability score (0.17) and the second least favorable synthetic accessibility score (4.88). In contrast, compound E obtained the same bioavailability score as the top-scoring compounds A and C (0.55) but received the least favorable synthetic accessibility score (5.35). Compound B is the largest molecule with complex ring structures, likely compromising its bioavailability score. In turn, compound E, despite being a molecule with only a simple quinone ring, has a long chain, which hinders its synthetic accessibility without altering its bioavailability.

Analysis with BioNavi-NP provided further insights into the compounds' molecular characteristics. Quinine, one of the control compounds, is synthesized from the amino acid tryptophan into tryptamine and then merged with secologanin to form strictosidine in quinoline alkaloid biosynthesis [46]. From the BioNavi-NP analysis, quinine revealed two synthesis intermediates, while the other control drug compound, IZP, was predicted to have nine synthesis intermediates. Notably, compounds D and E displayed the least intermediary compounds in their predicted biosynthesis pathway, resembling quinine's profile. Compounds A and C followed, with three intermediaries each. Finally, compound B exhibited the number of four intermediates. Compound E, being of an overall large size, is relatively simple, possibly due to its long chain bound to a single ring. In summary, compounds A and C emerge as the most promising drug candidates based on their favorable FMO electronic gaps and structural features contributing to bioavailability and synthetic accessibility.

4.2. Likely activity and protein interaction predictions

The PASS server predicted the likelihood of compound activity using a machine learning algorithm based on a database of over 300,000 organic compounds with known biological activities, categorized into 4,000 terms [47]. According to the predictions, none of the five compounds

showed higher antiprotozoal and antiplasmodial properties than quinine. However, compound E exhibited the closest resemblance, while compound A showed moderate similarity. Compounds B, C, and D did not exhibit these properties. The close resemblance in compound E is supported by the data from the National Center for Biotechnology Information, with the bioassay record showing that compound E (PubChem CID: 90665546) activity in *P. berghei*-infected mice reduced parasitemia at 25 mg/kg/day dosage (per oral; 4 days up to day 60) relative to control [48], being the only compound in the present study tested so far.

The SwissTargetPrediction tool predicted the proteins likely targeted by the compounds [28]. This approach aimed to identify compound similarities with the control drugs and other compounds by assessing shared enzyme targets. According to the predictions (Table 4), compound A was the only one sharing an enzyme target with quinine, while compounds C and D each shared one protein target with IZP. Interestingly, compound A also shared enzyme targets with compound C, which also shared targets with compound D. Thus, compounds A, C, and D were identified as the most promising candidates for further evaluation through molecular docking and dynamics tests to assess their activity against control drugs.

4.3. Molecular simulations

Molecular docking results indicated that compounds C and D exhibit superior binding affinities compared to the control drugs. During docking, compounds C and D formed interactions with more amino acid residues compared to the control drugs. IZP formed interactions with multiple residues, including various types of pi (π)-bonds, such as π-alkyl, π-π stack, and π-sigma/π-σ bonds. In addition to π- and hydrogen bonds, hydrophobic interactions also contributed to the strong binding between compound C and the amino acid residues. Compound C formed more interactions (including π-bonds, hydrogen bonds, and hydrophobic interactions) with the PNP amino acid residues than quinine. Larger molecules can establish more interactions during docking as they can access more residues within the catalytic pocket, likely explaining why compound D exhibited the second-largest binding affinity, after compound C, with PNP, while ranking third after compounds C and E. Compound D surpassed compound C in binding affinity for EMP1, possibly due to the larger contact area available in this protein.

Among all compounds, compound B emerged as the weakest candidate in molecular dynamics simulations, exhibiting notably high fluctuations in both DHODH and EMP1 during the 50 ns simulations (Fig. 4). In MM/PBSA testing, compounds C, D, and E exhibited the highest binding free energies (Fig. 5), indicating stronger interactions and bonds, which correlate positively with the docking binding affinity. The high binding free energy implies stronger interactions and bonds, correlating positively with docking binding affinity [49]. During molecular dynamics simulations, incorporating solvation and time-dependent dynamics, compound C overtook the other compounds regarding fluctuation stability with all proteins. In PNP, compound C exhibited shorter fluctuations than the baseline average RMSD of the protein.

4.4. Impact on natural compound-based antimalarial drug discovery

This study's findings hold significant implications for natural compound-based antimalarial drug discovery, offering promising avenues for future research and drug development. Natural compounds derived from plants have long been a valuable source of medicinal agents, and this study underscores their potential in combating malaria, which continues to pose a significant global health burden.

By harnessing the power of multiple tools, liquid chromatography-tandem mass spectrometry (LC-MS/MS) analysis combined with the *in-silico* data analysis, this study identified five quinone-derivative compounds from neem leaves, identifying compound C as superior to all other compounds, shedding light on its potential as an antimalarial drug. Other studies also applied similar methods to different malarial virulence factors [50, 51]. The findings in this study not only contribute to our understanding of the molecular mechanisms underlying antimalarial activity but also pave the way for the development of novel plant-based antimalarial drugs by characterizing them with novel tools, gaining insight into their roles and functions within their source organisms, *i.e.*, pathway characterization and target prediction. By leveraging the rich diversity of natural compounds and employing advanced computational methodologies, researchers can expedite the discovery and optimization of potent antimalarial agents using locally known plants. Furthermore, integrating traditional knowledge with modern scientific approaches holds promise for the sustainable utilization of medicinal plants in the fight against malaria. Given neem's established use in herbal medicine, compound C *in silico* profile adds to the evidence supporting plant-based antimalarial agents. Further studies on neem-derived compounds could contribute to sustainable, accessible therapies in malaria-endemic regions.

5. Conclusion

From 184 metabolites found in neem leaf extract using LC-MS, five compounds (A-E) were selected, and after a suite of in silico analyses with these five, compound C emerged as the most promising neem-derived antimalarial candidate. Compound C revealed favorable binding affinities (comparable to established antimalarials, PNP, and IZP in DHODH) in molecular docking and stability in molecular dynamics analyses, had the highest binding free energy among the top three compounds in MM/PBSA, and could also bind to EMP1. Compound C met LRo5 ADME criteria, revealing the same bioavailability as three other assessed compounds (0.55) and having reasonable synthetic accessibility. Biosynthetic pathway predictions determined that Compound C has three intermediates, whereas quinine and IZP have two and nine, respectively. Even though compound C has no predicted activity in antiprotozoal and antiplasmodial categories, it shared three enzyme targets with IZP in the target prediction assessments. These findings strongly support further *in vitro* and *in vivo* studies on compound C to validate its potential as a sustainable antimalarial treatment.

6. Acknowledgments

We acknowledge all Forensic Laboratory Center (PUSLABFOR) personnel at the National Police Headquarters (Bogor, Indonesia) for lending their hands during the LC-MS analysis. We also would like to thank Mr. Andi Baso Manguntungi for being a liaison between the authors (AH and MS) and the PUSLABFOR and especially thank Sabrina Nuha, Kharmila Rahmadani, Muhammad Faiz, and Muhammad Aziz K. for helping with sample collection and LC-MS data processing.

7. Conflict of interest

The authors have no conflict of interest to declare.

References

[1] Harijanto P. *Malaria*. 4 ed. Universitas Indonesia; 2006.

[2] WHO. *World Malaria Report*, 2022.

https://www.who.int/publications/i/item/9789240064898

[3] Visser BJ, Wieten RW, Kroon D, Nagel IM, Bélard S, van Vugt M, Grobusch MP. Efficacy and safety of artemisinin combination therapy (ACT) for non-falciparum malaria: a systematic review, *Malaria Journal*, 13(1): 463, 2014.

https://doi.org/10.1186/1475-2875-13-463

[4] Khuroo MS. Chloroquine and hydroxychloroquine in coronavirus disease 2019 (COVID-19). Facts, fiction and the hype: a critical appraisal, *International Journal of Antimicrobial Agents*, 56(3): 106101, 2020.

https://doi.org/10.1016/j.ijantimicag.2020.106101

[5] Erhunse N, Sahal D. Protecting future antimalarials from the trap of resistance: Lessons from artemisinin-based combination therapy (ACT) failures, *Journal of Pharmaceutical Analysis*, 11(5): 541-554, 2021.

https://doi.org/10.1016/j.jpha.2020.07.005

[6] Cui L, Su X-z. Discovery, mechanisms of action and combination therapy of artemisinin, *Expert Review of Anti-infective Therapy*, 7(8): 999-1013, 2009.

https://doi.org/10.1586/eri.09.68

[7] Gopalakrishnan AM, Kumar N. Antimalarial Action of Artesunate Involves DNA Damage Mediated by Reactive Oxygen Species, *Antimicrobial Agents and Chemotherapy*, 59(1): 317-325, 2015.

https://doi.org/10.1128/aac.03663-14

[8] Waingeh VF, Groves AT, Eberle JA. Binding of quinoline-based inhibitors to Plasmodium falciparum lactate dehydrogenase: a molecular docking study, *Open Journal of Biophysics*, 3(4): 2013.

https://doi.org/10.4236/ojbiphy.2013.34034

[9] Lalloo DG, Shingadia D, Bell DJ, Beeching NJ, Whitty CJM, Chiodini PL. UK malaria treatment guidelines 2016, *Journal of Infection*, 72(6): 635-649, 2016.

https://doi.org/10.1016/j.jinf.2016.02.001

[10] Thompson AJ, Lochner M, Lummis SCR. The antimalarial drugs quinine, chloroquine and mefloquine are antagonists at 5-HT3 receptors, *British Journal of Pharmacology*, 151(5): 666-677, 2007.

https://doi.org/10.1038/sj.bjp.0707238

[11] Cechinel-Filho V. *Plant bioactives and drug discovery: principles, practice, and perspectives*. John Wiley & Sons, 2012.

[12] Plant of The World Online. 2023.

https://powo.science.kew.org/taxon/urn:lsid:ipni.org:names:1213180-2

[13] Simatupang GMK LD, Ferdinal F, Yulianti E. Identifikasi fitokimia dan kapasitas total antioksidan daun mimba (*Azadirachta indica* A. Juss) serta uji toksisitasnya terhadap larva *Artemia salina* Leach, *Tarumanegara Medical Journal*, 5(1): 59-66, 2023.

[14] Udeinya JI, Shu EN, Quakyi I, Ajayi FO. An Antimalarial Neem Leaf Extract has Both Schizonticidal and Gametocytocidal Activities, *American Journal of Therapeutics*, 15(2): 108-110, 2018.

https://doi.org/10.1097/MJT.0b013e31804c6d1d

[15] White NJ, Pukrittayakamee S, Hien TT, Faiz MA, Mokuolu OA, Dondorp AM. Malaria, *The Lancet*, 383(9918): 723-735, 2014.

https://doi.org/10.1016/S0140-6736(13)60024-0

[16] Kokkonda S, El Mazouni F, White KL, White J, Shackleford DM, Lafuente-Monasterio MJ, Rowland P, Manjalanagara K, Joseph JT, Garcia-Perez A, Fernandez J, Gamo FJ, Waterson D, Burrows JN, Palmer MJ, Charman SA, Rathod PK, Phillips MA. Isoxazolopyrimidine-Based Inhibitors of *Plasmodium falciparum* Dihydroorotate Dehydrogenase with Antimalarial Activity, *ACS Omega*, 3(8): 9227-9240, 2018.

https://doi.org/10.1021/acsomega.8b01573

[17] Ichida K, Hosoyamada M, Hosoya T, Endou H. Chapter 38 - Primary Metabolic and Renal Hyperuricemia. In: Lifton RP, Somlo S, Giebisch GH, Seldin DW, editors. *Genetic Diseases of the Kidney*. San Diego: Academic Press; 651-660, 2009.

[18] Dziekan JM, Yu H, Chen D, Dai L, Wirjanata G, Larsson A, Prabhu N, Sobota RM, Bozdech Z, Nordlund P. Identifying purine nucleoside phosphorylase as the target of quinine using cellular thermal shift assay, *Science Translational Medicine*, 11(473): 2019.

https://doi.org/10.1126/scitranslmed.aau3174

[19] Lennartz F, Smith C, Craig AG, Higgins MK. Structural insights into diverse modes of ICAM-1 binding by *Plasmodium falciparum*-infected erythrocytes, *Proceedings of the National Academy of Sciences*, 116(40): 20124-20134, 2019.

https://doi.org/10.1073/pnas.1911900116

[20] Parikesit AA, Nurdiansyah R, Garrido G. Natural products repurposing of the H5N1-based lead compounds for the most fit inhibitors against 3C-like protease of SARS-CoV-2, *Journal of Pharmacy & Pharmacognosy Research*, 9(5): 730-745, 2021.

[21] Ayers M. ChemSpider: The Free Chemical Database, *Reference Reviews*, 26(7): 45-46, 2012.

https://doi.org/10.1108/09504121211271059

[22] Patai S, Rappoport Z. *The Quinonoid Compounds: Part 2*. John Wiley & Sons Ltd, 1988.

[23] Daina A, Michielin O, Zoete V. SwissADME: a free web tool to evaluate pharmacokinetics, drug-likeness and medicinal chemistry friendliness of small molecules, *Scientific Reports*, 7(1): 42717, 2017.

https://doi.org/10.1038/srep42717

[24] Lipinski CA, Lombardo F, Dominy BW, Feeney PJ. Experimental and computational approaches to estimate solubility and permeability in drug discovery and development settings, *Advanced Drug Delivery Reviews*, 46(1): 3-26, 2001.

https://doi.org/10.1016/S0169-409X(00)00129-0

[25] Martin YC. A Bioavailability Score, *Journal of Medicinal Chemistry*, 48(9): 3164-3170, 2005.

https://doi.org/10.1021/jm0492002

[26] Ertl P, Schuffenhauer A. Estimation of synthetic accessibility score of drug-like molecules based on molecular complexity and fragment contributions, *Journal of Cheminformatics*, 1(8), 2009.

https://doi.org/10.1186/1758-2946-1-8

[27] Zheng S, Zeng T, Li C, Chen B, Coley CW, Yang Y, Wu R. Deep learning driven biosynthetic pathways navigation for natural products with BioNavi-NP, *Nature Communications*, 13(1): 3342, 2022.

https://doi.org/10.1038/s41467-022-30970-9

[28] Daina A, Michielin O, Zoete V. SwissTargetPrediction: updated data and new features for efficient prediction of protein targets of small molecules, *Nucleic Acids Research*, 47(W1): W357-W364, 2019.

https://doi.org/10.1093/nar/gkz382

[29] Lagunin A, Stepanchikova A, Filimonov D, Poroikov V. PASS: prediction of activity spectra for biologically active substances, *Bioinformatics*, 16(8): 747-748, 2000.

https://doi.org/10.1093/bioinformatics/16.8.747

[30] Frisch M, Trucks G, Schlegel H, Scuseria G, Robb M, Cheeseman J, Scalmani G, Barone V, Mennucci B, Petersson GA. *Gaussian 09*. Wallingford, CT, USA: Gaussian Inc. 2013.

[31] Hanwell MD, Curtis DE, Lonie DC, Vandermeersch T, Zurek E, Hutchison GR. Avogadro: an advanced semantic chemical editor, visualization, and analysis platform, *Journal of Cheminformatics*, 4(17), 2012.

https://doi.org/10.1186/1758-2946-4-17

[32] O'Boyle NM, Banck M, James CA, Morley C, Vandermeersch T, Hutchison GR. Open Babel: An open chemical toolbox, *Journal of Cheminformatics*, 3(33), 2011.

https://doi.org/10.1186/1758-2946-3-33

[33] Becke AD. Density-functional exchange-energy approximation with correct asymptotic behavior, *Physical Review A*, 38(6): 3098-3100, 1988.

https://doi.org/10.1103/PhysRevA.38.3098

[34] Lee C, Yang W, Parr RG. Development of the Colle-Salvetti correlation-energy formula into a functional of the electron density, *Physical Review B*, 37(2): 785-789, 1988.

https://doi.org/10.1103/PhysRevB.37.785

[35] Trott O, Olson AJ. AutoDock Vina: Improving the speed and accuracy of docking with a new scoring function, efficient optimization, and multithreading, *Journal of Computational Chemistry*, 31(2): 455-461, 2010.

https://doi.org/10.1002/jcc.21334

[36] Abraham MJ, Murtola T, Schulz R, Páll S, Smith JC, Hess B, et al. GROMACS: High performance molecular simulations through multi-level parallelism from laptops to supercomputers, *SoftwareX*, 1-2: 19-25, 2015.

https://doi.org/10.1016/j.softx.2015.06.001

[37] Valdés-Tresanco MS, Valdés-Tresanco ME, Valiente PA, Moreno E. gmx_MMPBSA: A New Tool to Perform End-State Free Energy Calculations with GROMACS, *Journal of Chemical Theory and Computation*, 17(10): 6281-6291, 2021.

https://doi.org/10.1021/acs.jctc.1c00645

[38] Hou T, Wang J, Li Y, Wang W. Assessing the Performance of the MM/PBSA and MM/GBSA Methods. 1. The Accuracy of Binding Free Energy Calculations Based on Molecular Dynamics Simulations, *Journal of Chemical Information and Modeling*, 51(1): 69-82, 2011.

https://doi.org/10.1021/ci100275a

[39] Huang S-Y. Comprehensive assessment of flexible-ligand docking algorithms: current effectiveness and challenges, *Briefings in Bioinformatics*, 19(5): 982-994, 2017.

https://doi.org/10.1093/bib/bbx030

[40] Rahmah Z, Nirmala KC, Nashichuddin A, Riskiyana R, Milliana A, Indriana N, Fitria L, Ayudianti P, Kholil M. Effect of neem leaf extract (*Azadirachta indica*) in reducing the degree of parasitemia and apoptosis in C57BL mice with cerebral malaria, *Veterinary World*, 17(7): 1497, 2024.

[41] Indriana N, Kustiawan NS, Milliana A, Rahmah Z, Nashichuddin A, Pagalay U, Wulan P, Kusuma YI, Kholil M. Effect of neem leaf therapy (*Azadirachta indica*) on TNF-α expression and hepatocyte apoptosis of balb/c mice infected with *Plasmodium berghei* anka, *GSC Biological and Pharmaceutical Sciences*, 25(2): 283-292, 2023.

[42] Rahmah Z, Arif CH, Milliana A, Indriana N, Nashichuddin A. Prevention of Cerebral Malaria Hypoxia through administration of Neem leaves extract (*Azadirachta indica*) in Mice C57BL. *Research Journal of Pharmacy and Technology*, 17(1), 2024.

[43] Igwenyi IO, Onodugo CA, Aja PM, Elom SO, Awoke JN, Ibhadode OS, Uraku AJ, Nzubechukwu E, Obasi AN, Ebuka ED, Igwenyi IP, Ogbu PN, Egwu C, Atoki AV. *Azadirachta indica* fruit juice clears malaria parasites and replenishes blood levels in *Plasmodium berghei*-infected mice, *Phytomedicine Plus*, 4(4): 100615, 2024.

https://doi.org/10.1016/j.phyplu.2024.100615

[44] Hagar M, Ahmed HA, Aljohani G, Alhaddad OA. Investigation of Some Antiviral N-Heterocycles as COVID 19 Drug: Molecular Docking and DFT Calculations, *International Journal of Molecular Sciences*, 21(11): 3922, 2020.

[45] Price G, Patel DA. Drug Bioavailability, *StatPearls Publishing*, Treasure Island (FL), 2023.

[46] Geerlings A, Hallard D, Martinez Caballero A, Lopes Cardoso I, van der Heijden R, Verpoorte R. Alkaloid production by a *Cinchona officinalis* 'Ledgeriana' hairy root culture containing constitutive expression constructs of tryptophan decarboxylase and strictosidine synthase cDNAs from *Catharanthus roseus*, *Plant Cell Reports*, 19(2): 191-196, 1999.

https://doi.org/10.1007/s002990050732

[47] Filimonov DA, Lagunin AA, Gloriozova TA, Rudik AV, Druzhilovskii DS, Pogodin PV, Poroikov VV. Prediction of the Biological Activity Spectra of Organic Compounds Using the Pass Online Web Resource, *Chemistry of Heterocyclic Compounds*, 50(3): 444-457, 2014.

https://doi.org/10.1007/s10593-014-1496-1

[48] National Center for Biotechnology Information: PubChem Bioassay Record for AID 1118191, Source: ChEMBL, 2024.

https://pubchem.ncbi.nlm.nih.gov/bioassay/1118191

[49] Al-Khafaji K, Al-Duhaidahawi D, Taskin Tok T. Using integrated computational approaches to identify safe and rapid treatment for SARS-CoV-2, *Journal of Biomolecular Structure and Dynamics*, 39(9): 3387-3395, 2020.

https://doi.org/10.1080/07391102.2020.1764392

[50] Hameed A, Masood S, Hameed A, Ahmed E, Sharif A, Abdullah MI. Anti-malarial, cytotoxicity and molecular docking studies of quinolinyl chalcones as potential anti-malarial agent, *Journal of Computer-Aided Molecular Design*, 33(7): 677-688, 2019.

https://doi.org/10.1007/s10822-019-00210-2

[51] Patel AJ, Patel MP, Dholakia AB, Patel VC, Patel DS. Antitubercular, Antimalarial Activity and Molecular Docking Study of New Synthesized 7-Chloroquinoline Derivatives, *Polycyclic Aromatic Compounds*, 42(7): 4717-4725, 2022.

https://doi.org/10.1080/10406638.2021.1909082

Bioprospección *in silico* de alcaloides derivados de quinina con potencial antimalárico en neem (*Azadirachta indica*)

Resumen: La malaria, causada por el protozoo *Plasmodium* spp. y transmitida por mosquitos *Anopheles*, sigue siendo una amenaza significativa para la salud a nivel mundial. Con la aparición de cepas resistentes a la cloroquina, es urgente encontrar tratamientos alternativos basados en compuestos naturales. Este estudio explora el neem (*Azadirachta indica*), una planta del sudeste asiático, como fuente de agentes antimaláricos. Mediante un análisis de Cromatografía Líquida-Espectrometría de Masas en Tándem (LC-MS/MS) de un extracto de hojas de neem, se identificaron 184 compuestos, de los cuales cinco derivados de quinona fueron evaluados *in silico* contra tres proteínas de virulencia de *Plasmodium falciparum*: fosforilasa de nucleósidos de purina (PNP), dihidroorotato deshidrogenasa (DHODH) y la proteína de membrana eritrocitaria 1 (EMP1). Entre estos cinco compuestos (A-E), el compuesto C se destacó como el mejor candidato, obteniendo una alta clasificación en estabilidad molecular (brechas de energía FMO), parecido a fármaco (Regla de los 5 de Lipinski), biodisponibilidad y accesibilidad sintética. Además, el compuesto C presentó una fuerte afinidad de unión con PNP y DHODH en los estudios de acoplamiento molecular y simulaciones dinámicas, y se ubicó entre los tres primeros en cuanto a energía libre de unión en los cálculos MM/PBSA. Sin embargo, no mostró actividad antiprotozoaria en la evaluación PASS, a pesar de compartir objetivos enzimáticos clave con fármacos antimaláricos establecidos. Estos hallazgos sugieren que el compuesto C es un candidato prometedor para futuras investigaciones como posible agente antimalárico.

Palabras Clave: Bioinformática; derivados de quinina; metabolito secundario; predicción de rutas; prospección de fármacos antimaláricos.

Bioprospecção *in silico* de alcaloides derivados da quinina com potencial antimalárico no neem (*Azadirachta indica*)

Resumo: A malária, causada pelo protozoário *Plasmodium* spp. e transmitida por mosquitos *Anopheles*, continua sendo uma ameaça significativa à saúde global. Com o surgimento de cepas resistentes à cloroquina, é urgente encontrar tratamentos alternativos baseados em compostos naturais. Este estudo explorou o neem (*Azadirachta indica*), uma planta do Sudeste Asiático, como fonte de agentes antimaláricos. Por meio de uma análise de Cromatografia Líquida-Espectrometria de Massas em Tandem (LC-MS/MS) de um extrato de folhas de neem, foram identificados 184 compostos, dos quais cinco derivados de quinona foram avaliados *in silico* contra três proteínas de virulência de *Plasmodium falciparum*: fosforilase de nucleosídeos de purina (PNP), diidroorotato desidrogenase (DHODH) e proteína de membrana eritrocitária 1 (EMP1). Entre esses cinco compostos (A-E), o composto C se destacou como o melhor candidato, obtendo uma alta classificação em estabilidade molecular (diferenças de energia FMO), semelhança com fármacos (Regra dos 5 de Lipinski), biodisponibilidade e acessibilidade sintética. Além disso, o composto C apresentou forte afinidade de ligação com PNP e DHODH nos estudos de acoplamento molecular e simulações dinâmicas, posicionando-se entre os três primeiros em termos de energia livre de ligação nos cálculos MM/PBSA. No entanto, o composto não demonstrou atividade antiparasitária na avaliação PASS, apesar de compartilhar alvos enzimáticos chave com medicamentos antimaláricos já estabelecidos. Esses achados sugerem que o composto C é um candidato promissor para futuras pesquisas como um possível agente antimalárico.

Palavras-chave: Bioinformática; derivados de quinina; metabólito secundário; predição de rotas; prospecção de fármacos antimaláricos.

Alfin Hidayat

Alfin Hidayat studied drug discovery at Universitas Teknologi Sumbawa, Indonesia. For his thesis, he focused on neem (Azadirachta indica) and its potential against malaria. His research involved bioinformatics analyses, including chromatography data interpretation and protein-ligand interaction studies through molecular docking and molecular dynamics simulations. These approaches were essential for identifying bioactive compounds and understanding their mechanisms of action, contributing to the development of potential antimalarial drugs from natural sources.

ORCID: -

Mamat Sugianto

Mamat Sugianto pursued drug discovery studies at Universitas Teknologi Sumbawa, Indonesia. His research centered on Melaleuca leucadendra-derived compounds, utilizing bioinformatics for chromatography analysis and protein-ligand interaction studies, such as molecular docking and dynamics. Additionally, he explored drug discovery targeting human papillomavirus (HPV) using computational approaches, including drug prediction and molecular modeling techniques. His work highlighted the potential of natural products and in silico methods in accelerating drug development processes.

ORCID: -

Ali Budhi Kusuma

Dr. Ali Budhi Kusuma is an expert in microbiology with extensive experience in extremophile microbes and parasitology, focusing primarily on malaria research. He serves as a senior lecturer at Universitas Teknologi Sumbawa, Indonesia, where he mentors students in microbiological sciences. Beyond academia, Dr. Kusuma actively participates in Access and Benefit Sharing (ABS) initiatives under the United Nations Environment Programme (UNEP) for Timor Leste, supporting the implementation of the Convention on Biological Diversity.

ORCID: 0000-0002-0243-9514

Lili Suharli

Lili Suharli is a lecturer at Universitas Teknologi Sumbawa, Indonesia, specializing in biotechnology with interests spanning plant sciences, entomology, and microbiology. Her current research focuses on developing seaweed-based plant fertilizers to enhance crop productivity, particularly in Sumbawa. By exploring the applications of natural marine resources in sustainable agriculture, she aims to improve soil health, boost crop yields, and promote environmentally friendly farming practices that benefit local agricultural communities.

ORCID: 0000-0002-0209-3154

Adhityo Wicaksono

Dr. Adhityo Wicaksono is a Bioinformatics Research Fellow at Genomik Solidaritas Indonesia (GSI) Lab, Jakarta. His expertise lies in plant molecular biology and bioinformatics, with research spanning functional omics analyses of Rafflesiaceae parasitic plants, abiotic stress responses in crops, and model organism Arabidopsis thaliana. In addition to omics studies, he has published work on plant-based compound drug discovery, employing computational techniques like molecular docking and systems biology approaches to identify potential bioactive compounds.

ORCID: 0000-0003-3298-3577